SOL Effects on the Pedestal Structure in DIII-D Discharges

A.C. Sontag[1], X. Chen[2], J. Canik[1], A. Leonard[2], J.D. Lore[1], A.L. Moser[2], M. Murakami[1], J.M. Park[1], C. Petty[2]

[1]Oak Ridge National Laboratory, Oak Ridge, TN, USA

[2]General Atomics, La Jolla, CA, USA

E-mail contact of main author: sontagac@ornl.gov

This manuscript has been authored by UT-Battelle, LLC under Contract No. DE-AC05-00OR22725 with the U.S. Department of Energy. The United States Government retains and the publisher, by accepting the article for publication, acknowledges that the United States Government retains a non-exclusive, paid-up, irrevocable, world-wide license to publish or reproduce the published form of this manuscript, or allow others to do so, for United States Government purposes. The Department of Energy will provide public access to these results of federally sponsored research in accordance with the DOE Public Access Plan (http://energy.gov/downloads/doe-public-access-plan).

Abstract. SOLPS analysis explains the differences in pedestal structure associated with different ion ∇B drift directions in DIII-D. Core transport models predict that fusion power scales roughly as the square of the pressure at the top of the pedestal, so understanding the effects that determine pedestal structure in steady-state operational scenarios is important to projecting scenarios developed in DIII-D to ITER and other devices. Both experiments and modeling indicate that scrape off layer (SOL) conditions are important in optimizing the pedestal structure for high-beta steady-state scenarios. The SOLPS code is used to provide interpretive analysis of the pedestal and SOL to examine the nature of flows and fueling on the pedestal structure including the effects of drifts in the fluid model. This analysis shows that flows driven by the ion ∇B drift are outward when this drift is toward the x-point in a single-null divertor configuration (favorable ∇B direction for reduced H-mode power threshold), and inward when the drift is away from the x-point (unfavorable ∇B direction). It is hypothesized that these flows decrease the density gradient in the pedestal in the favorable direction, thereby stabilizing the kinetic ballooning mode (KBM) and increasing the pedestal width. Comparisons of pedestal structures in similarly shaped DIII-D steady-state plasmas confirm this change, showing increased density pedestal width and lower peak density and lower separatrix density with the favorable drift direction. The pedestal temperature is higher in the lower density case, resulting in an increased pedestal pressure, which indicates that the increased particle flux does not significantly degrade energy confinement. Modeling of cases with constant ∇B drift direction but changing between the more open lower divertor and more closed upper divertor show that there is increased fueling inside the pedestal with the more open geometry. The pedestal fueling rate for both attached and detached cases is always lower with more closed divertor geometry than in any cases with more open geometry.

1. Introduction

A high-priority goal for present operational scenario development experiments on the DIII-D [1] tokamak is to identify edge operational regimes with high performance, i.e. high pedestal pressure, which also maintain acceptable heat loads on plasma facing components (PFCs). Pedestal scaling is particularly critical in developing steady-state scenarios for future devices where the pressure gradient in the pedestal contributes significantly to the bootstrap current since increased bootstrap current leads to reduced external current drive requirements. The EPED model [2] is a tool for predicting the edge pedestal structure in ELMy H-mode discharges, which uses both peeling-ballooning and kinetic ballooning stability models to

predict the pedestal height and width. While this provides a good initial prediction, the limited physics included in this model leads to significant uncertainty in the predicted pedestal structure. The core fusion power is very sensitive to the pedestal pressure [3], so accurate prediction of the pedestal structure is required to model the fusion gain of future devices. Recent work on both ASDEX [4] and JET [5] indicate that modifications of the scrape-off layer density can have significant effects on the pedestal pressure.

An experiment was performed on DIII-D with the aim of optimizing the pedestal structure in steady-state scenarios. Similar discharges with opposite orientation of the ∇B drift direction to the x-point have been observed to have a significant change in the pedestal structure as shown in Figure 1. The discharge characteristics as well as the pedestal profile fitting are discussed in more detail in section 2.1. Figure 1 shows two steady-state scenario discharges with similar core confinement, but significantly different core pressures due to a change in the pedestal height. This effect was originally observed going from older discharges with an ITER similar shape, but unable to be sustained non-inductively due to B_T in the opposite direction as the plasma current, to a modified shape to better utilize the lower divertor pumping duct and reversed B_T to maximize current drive efficiency of off-axis NBI. This change in toroidal field caused the ion B×∇B drift direction to be away from the x-point (unfavorable direction for H-mode transition), and a 20% reduction in the pedestal pressure was observed. These discharges also had differences in shape and pumping due to changes in the location of the outer strike point. Subsequent experiments produced the discharges shown in Figure 1, which do not have the shape differences between the two ∇B drift directions. These experiments verified in both upper and lower single null configurations that ~10% higher pedestal pressure is obtained when the ion ∇B drift direction is toward the x-point. In the remainder of this paper, ∇B toward the x-point is referred to as the favorable direction, while ∇B away from the x-point is referred to as the unfavorable direction. In addition to the difference in pedestal height a wider density pedestal is observed with favorable ∇B drift direction.

The physics included in EPED is not specific to toroidal field direction, so it is not expected to predict this change in pedestal height. A number of DIII-D discharges with ITER similar shape that were optimized for high non-inductive current fraction were compared to their EPED1 predicted pedestal heights, and the model predictions agree within error, as shown in Figure 2. The dashed lines represent a 20% uncertainty window. Since the fusion gain is so sensitive to the pedestal pressure, it is necessary to understand how the toroidal field direction affects the pedestal structure within these error bars. It is hypothesized that flows driven by drift effects may be responsible for the pressure difference. The effects of divertor geometry as well as pumping and fueling differences will also affect the scrape-off layer (SOL) conditions, which can then impact the pedestal structure. To understand the effects of drifts, fueling and divertor geometry on the pedestal structure, the SOLPS 5.0 code [6] and the SOLPS-ITER code [7,8] have been used to model a number of discharges with varying ∇B drift direction and divertor geometry.

This paper will present modeling of discharges from two different experiments in order to determine which effects are causing the variation in the pedestal structure. Section 2 describes the modeling of high-performance steady-state discharges, with the favorability of the ∇B drift direction changed by going between upper single null (USN) and lower single null (LSN) magnetic configurations. These discharges all maintain B_T in the same direction as the plasma current in order to maximize off-axis neutral beam current drive efficiency [9]. These modeling results include the effects of ∇B drift induced flows to determine their effect on the pedestal structure. Section 3 describes modeling of discharges from an experiment designed to specifically isolate divertor geometry and fueling effects to determine how these affect the pedestal structure. The ∇B drift direction was held constant in the favorable direction for all of these discharges as density scans were performed to determine changes in the deuterium ionization and pedestal structure with changes in divertor geometry. The constant ∇B drift direction for these discharges eliminates any pedestal differences due to ∇B drift induced flows. Section 4 will summarize the results of both the ∇B drift and divertor closure effects on the pedestal structure.

2. SOLPS-ITER Modeling of Drift Effects in High-Performance Plasmas

To understand how drifts affect the pedestal structure in high-performance discharges, the high-performance, stationary phases of several DIII-D advanced scenario discharges have been modeled using the SOLPS-ITER code. SOLPS-ITER is a code suite that couples a fluid code for the ions to a Monte-Carlo code for the neutral species. B2.5 is the fluid code that solves Braginskii-like equations for the ions and electrons and EIRENE is the Monte-Carlo code that solves for the kinetic neutrals. The codes are coupled via source terms.

This comparison will focus on a particular set of matched discharges, one USN and one LSN, but otherwise geometrically similar plasmas, shown in Figure 1. The toroidal field direction was held constant for these two discharges so that the USN case (161605) has the ∇B drift direction toward the x-point (favorable ∇B drift), while the LSN case (161599) has the ∇B drift direction away from the x-point (unfavorable ∇B drift). While both configurations have the outer strike point near the entrance to the pump duct, there are differences in the divertor geometry between these two configurations, and the effects of the change in divertor geometry on the pedestal will be examined in section 3.

2.1. Plasma and Pedestal Characteristics

The discharges were analyzed during approximately stationary high performance conditions, with $\beta_N = 2.9$, as shown in Figure 3. The injected power was modulated for these discharges to control β_N. The pedestal profiles were determined over the last 20% of the ELM cycle during the quasi-stationary time window of 3.8 s to 4.2 s using the standard procedure previously developed at DIII-D [10]. All Thomson scattering measurements of electron density and temperature and CER measurements of the ion temperature that fall within the designated portion of the ELM cycle during this time window were mapped to normalized flux space for the profile fits. An example of the fit electron pressure profiles and the experimental data for the two shots being examined are shown in Figure 4. The profile evolution was examined for several discharges in this dataset and it was found that the

pedestal parameters had recovered to within 90% of their pre-ELM values within the first 20% of the ELM cycle, so these profiles represent the typical inter-ELM conditions.

A comparison of the ELM-synched profiles for these two shots is shown in Figure 5. The unfavorable ∇B case leads to lower temperature as shown in Figure 5(a). The decreased temperature in the case with unfavorable ∇B is due to increased ion and electron density in the pedestal. The unfavorable ∇B case also has an increased density gradient (reduced density pedestal width) compared to the favorable ∇B case, as shown in Figures 5(b) and 5(c). The separatrix density is increased also, indicating an outward shift of the density profile. The outward shift in the density profile is similar to that observed on ASDEX Upgrade associated with high field side high density discharges [11,12], while NSTX has observed an inward shift due to significant reductions in recycling [13,14]. The carbon concentration is increased in the favorable ∇B case, as shown in Figure 5(d), which contributes to the decreased ion density shown in Figure 5(c). Other than effects due to changes in divertor geometry, which will be discussed in section 3, the pumping and fueling for these two discharges is similar.

2.2. Drift Effects Modeling and Impact on Pedestal Structure

SOLPS-ITER was used for this modeling in order to include drift effects. Earlier versions of SOLPS used a numerical formulation for the drifts that experienced numerical instability in plasmas with an H-mode edge pedestal. SOLPS-ITER uses a new formulation with greatly increased stability in cases including drift effects, which allows for analysis of these effects in the high-performance DIII-D cases presented in this section. Drift effects are included by slowly increasing a numerical multiplier in the input in order to prevent numerical instabilities that can easily be driven by strong parallel gradients from the drifts.

The SOLPS simulations are run over the domain of $\psi_N = 0.8$ to the wall. The core electron density boundary condition is set to a fixed density at the measured value, while the core electron and ion power fluxes are each set to half of the total measured input power minus the measured radiated power in the core. The simulations are relatively insensitive to the exact power split between the ions and electrons since the radial energy transport coefficients for both species are adjusted to match the experimental profiles. Since the upstream profiles are matched to the experimental data, any increase or decrease in the power flux will only affect the target conditions and are not relevant to this study. Sheath boundary conditions are used at the target for the density and ion and electron energy and momentum equations. The region outside the last scrape-off-layer flux surface is treated as vacuum. The simulations described in this section only include deuterium. As particle balance was not a focus of these simulations, external gas puffing and pumping were not included in the simulations.

The anomalous cross-field transport coefficients are adjusted in SOLPS to match the model profiles with the experimental profiles to within the error of the experimental profile fits. Since the core density is fixed and this study was focused on particle flow dynamics rather than on total particle balance, no external fueling was included. The code adjusts the core particle flux to maintain the proscribed core density boundary condition. Typical model output profiles with the drifts turned off and ELM-averaged experimental data using the last

20% of the ELM cycle are shown in Figure 6. Since the CER T_i measurements are sparse outside the last closed flux surface, an exponential fall off from the separatrix is assumed.

Figure 7 shows the effects of the *∇B* drift on the particle flow for a deuterium only case with the *∇B* drift multiplier at 0.8, comparing both favorable and unfavorable *∇B* drift direction for shot 161599. The radial flow velocity driven by the ∇B drift at the midplane changes sign from positive (radially inward) when the *∇B* drift is away from the x-point, to negative (radially outward) when the *∇B* drift is towards the x-point. Figure 8 (a) shows the total radial particle flux, which includes the *∇B* driven flows, for both field directions in comparison to the case with no drift flows. Positive values indicate inward flux while negative values indicate outward flux. The transport coefficients are the same for all 3 cases, so that the SOLPS profiles in the no drift case match the experimental profiles, while the cases with *∇B* drift effects show significant deviation from the experimentally measured density and temperature profiles, as shown in Figure 8 (b). It is hypothesized that the increased outward particle flux in the favorable ∇B case predicted by the SOLPS modeling results in a larger density pumpout inside the separatrix, and is responsible for the experimentally observed decreased density gradient in the pedestal. A decreased density gradient would stabilize the KBM and allow the experimentally observed greater pedestal width.

The modeling performed in this section does not account for the changes in the divertor geometry in the experimental results and how that may affect the pedestal structure when changing from an upper single null geometry to a lower single null geometry. In order to determine if the divertor geometry is changing the fueling and/or the pumping for these discharges, discharges from a second experiment are modeled and discussed in section 3.

3. SOLPS Modeling of Divertor Geometry and Fueling Effects

Divertor geometry is known to have a strong influence on the particle sources/sinks in the divertor region and at the plasma edge [15]. Divertor closure is increased by aligning the physical geometry of the divertor components with the magnetic geometry so that there is a reduced conductance for neutral backflow from the divertor target into the main chamber. This can affect the degree of neutral penetration across the separatrix, changing the particle source in the pedestal. High closure is desirable for achieving radiative divertor conditions that reduce the heat and particle fluxes to plasma facing components, but the effects of divertor closure on the pedestal structure are under investigation. Ensuring that a divertor design which is favorable for maintaining acceptable target heat loads is compatible with maintaining a high-performance AT core plasma is highly desirable [16].

To examine the effects of divertor closure on the plasma fueling and pedestal structure, a series of discharges with three different plasma geometries has been modeled using SOLPS 5.0. The experimental results for the discharges in this study have been reported in [17,[18]] The geometries are shown in Figure 9. The divertor geometries range from the most open case with the outer strike point on the shelf above the pump duct, to the most closed case when the upper divertor is used. The case with the outer strike point on the floor in front of the pump duct is of intermediate closure. Increased closure results in a lower fraction of the neutrals recycled from the target escaping the divertor region. The *∇B* drift direction was always

towards the x-point, or in the favorable direction, for these cases. The constant ∇B drift direction removed the possibility of differences in the pedestal structure due to this effect, so the ∇B drift multiplier was set to zero for these simulations. This results in a significant decrease in the time required to converge each simulation, which allows the pedestal structure to be matched for each discharge examined. Other than the location of the outer strike point, the magnetic geometries were matched as closely as possible, including the length of the outer leg of the separatrix. This required the discharge with the outer strike point on the shelf to be shifted vertically.

Density scans were performed for these experiments by puffing large amounts of gas, in the range of $3x10^{20}$ to $6x10^{21}$ particles/s, with some cases reaching detachment. These cases were modeled using deuterium and carbon as the plasma species. All carbon in the simulation is sourced from target sputtering. The core deuterium fueling rate was obtained from simulations using the ONETWO core transport code [19], and the core particle flux was used as a boundary condition. Other boundary conditions are the same as described in section 2.2. To model the divertor cryopump, a surface with reflection coefficient of 0.6 was placed at the opening of the pump duct [20,21]. The large gas puff source used to vary density was included near the actual source location and the measured experimental flow rates were used in the simulation. The gas puff for the upper single null configuration was at the bottom of the machine and the gas puff for the shelf and floor lower single null configurations was at the top of the machine. In order to successfully generate the model grid for the floor configuration, the top corner of the shelf was removed over the entrance to the pump duct, creating an angled surface which decreases the closure for the model as compared to the actual in-vessel construction.

The effects of divertor closure can be seen by looking at the SOLPS calculated neutral density in the poloidal plane, as shown in Figure 10. The most open configuration with the outer strike point on the shelf, shown in Figure 10 (a), allows the recycled neutrals to spread through the vessel, with significant density extending well above the midplane. The intermediate closure of the floor configuration, shown in Figure 10 (b), traps many of the neutrals in the divertor region and increases the peak neutral density in this region. The most closed upper single null configuration, shown in Figure 10 (c) traps most of the recycled neutrals in the divertor and increases the peak neutral density by several orders of magnitude. The effectiveness of the pumping in the divertor region will be increased by this increased neutral trapping. These results are consistent with recent modeling of highly closed divertors on DIII-D [22].

Of greatest interest to this study is how this neutral trapping affects the pedestal fueling in DIII-D. The poloidal cross section of the SOLPS calculated deuterium ionization rate is shown in Figure 11. In the open divertor shelf configuration shown in Figure 11 (a), the peak ionization rate is lower and there is significant ionization throughout the vessel and inside the last closed flux surface. The more closed configurations shown in Figures 11 (b) and (c) keep the ionization more localized to the target regions.

The change in ionization location due to detachment is evident in Figure 12, which shows the SOLPS modeled ionization for the detached case in the floor configuration. When the plasma is attached, as shown in Figure 11 (b), nearly all of the ionization occurs at the targets, near

the strike points. During detachment, there is a gap between the ionization front and the target, as shown in Figure 12. The shift in the ionization off of the target creates a particle source that is much more spatially distributed and of lower local intensity. The peak ionization rate at the target for the attached case is ~ 1e27 particles/m^3/s, while the peak ionization rate for the detached case is ~ 1e25 particles/m^3/s.

Both the divertor geometry and the upstream density impact the deuterium ionization rate profile, as shown in Figure 13. This figure shows the poloidally averaged deuterium ionization rate profile for all of the magnetic configurations in both (a) attached and (b) detached cases. The average is performed from x-point to x-point in the computational domain, so does not extend to the targets where most of the ionization occurs. In all of the magnetic configurations, the peak magnitude of the ionization rate increases by at least a factor of 2 with the onset of detachment due to decreased ionization rate at the targets with detachment. In both of the cases with increased divertor closure, the ionization rate peaks outside of the separatrix, while in the shelf configuration the ionization rate peaks just inside the separatrix. In both the attached and detached cases, the peak ionization rate for the USN configuration is much higher than both the floor and shelf configurations.

The distributed ionization source resulting from detachment shifts much of the ionization near the separatrix, but the fraction of ionization that occurs within the last closed flux surface compared to outside in the SOL is fairly constant over the density scans as shown in Figure 14. The fraction ionized within the core ($\psi_N < 1$) for the shelf configuration is consistently 4-5 times greater than the fraction ionized within the core for the floor and USN configurations. The shot shown in Figure 12 is represented in Figure 14 by the black circle at a density of ~2.2. There is a 0.07 decrease in the fraction ionized within the core between these two cases, but the overall dataset does not indicate a strong trend. The increased core fueling for the shelf configuration represents a source difference, primarily in the pedestal. However this does not contribute to the increased pedestal density in the lower single null high performance cases with reversed B_T (unfavorable drift direction) discussed in section 2, as these discharges used the floor configuration. Also the increased fueling just outside the separatrix does not appear to be affecting the pedestal significantly in the high performance discharges, as these discharges have reduced separatrix density. The difference in the pedestal density profile between the shelf and floor configurations is shown in Figure 15. Both of these discharges are attached with no added gas puffing. The difference in fueling just inside the separatrix is apparent as the shelf case has a steeper density gradient with a flat density inside of $\psi_N \sim 0.95$, while the floor case has a significant gradient inside of the knee in the density pedestal. Recent work has shown that the formation of a poloidally localized high density region in the high-field side scrape-off-layer may be due to drifts and could have a large impact on plasma fueling [23]. The simulations in this study at high density did not include drifts, so a study of the pedestal fueling with drifts included in the simulations is planned for future work.

4. Summary of SOLPS Modeling of Fueling and Drift Effects on Pedestal Structure

SOLPS modelling indicates that ∇B drift driven currents increase the inward particle flux in the pedestal when the ∇B drift is away from the x-point and decrease the inward flux when the ∇B drift is toward the x-point. This change in flux coincides with a change in the density pedestal structure. When the ∇B drift is toward the x-point, the pedestal is wider with lower

n_e, but higher T_e, that allows it to achieve greater total pressure. This is consistent with the physics model of EPED, which relies on the physics that determines the stability thresholds for peeling-ballooning and kinetic ballooning modes to determine the pedestal height and width. EPED requires density as an input parameter and this work helps to understand how to set that parameter. The ∇B driven flows can affect the trajectory of the pedestal growth in stability space, achieving the same final pressure but altering the ratio of n_e/T_e. Favorable ∇B drift leads to increased outward particle flux in the pedestal, allowing T_e to rise more quickly than in the unfavorable ∇B drift case, while the density pedestal grows wider with favorable ∇B drift. Further study is required to determine if adjusting the input separatrix density for EPED based on the ∇B drift direction will reduce the error in EPED predictions.

The cases used for this profile comparison also have a change in divertor geometry when going from LSN to USN, however both cases have the outer strike point near the opening of the pump duct where there is some divertor closure. Modeling of divertor geometry effects indicates that both of the configurations have enough divertor closure to have similar pedestal fueling, so the differences in pedestal structure are due to the ∇B drift driven flows and the resulting effects on stability.

This work indicates that to achieve the highest pedestal pressure, plasmas should be run with the ion ∇B drift toward the x-point. It should be noted that at higher pressure, the poloidally localized high density structures formed by drift effects [23] may complicate this picture. High performance discharges with detached divertors will need to be produced and analyzed to determine which drift direction is optimal. In addition, ExB drift effects will be included in future work, but this will also include matching the rotation profile well to obtain an accurate representation of the radial electric field. Divertor geometry should not have significant impact on pedestal fueling as long as there is enough divertor closure and pumping to prevent significant neutral penetration across the last closed flux surface. The amount of pedestal fueling due to neutral penetration remains nearly constant even as the density is raised to achieve detachment, indicating that achieving high-performance AT operation with a detached divertor is possible. The caveat that this work was performed in a carbon wall machine with a high level of intrinsic radiation should be noted.

Acknowledgements

Work supported by US DOE under DE-AC05-00OR22725 and DE-FC02-04ER54698.

---

[1] LUXON, J. L., "A design retrospective of the DIII-D tokamak", Nucl. Fusion **42** (2002) 614.

[2] SNYDER, P.B, *et al*., "A first-principles predictive model of the pedestal height and width: development, testing and ITER optimization with the EPED model", Nucl. Fusion **51** (2011) 103016.

[3] KINSEY, J.E., *et al*., "Burning plasma projections using drift-wave transport models and scalings for the H-mode pedestal", Nucl. Fusion **43** (2003) 1845.

[4] DUNNE, M., *et al*., Plas. Phys. Cont. Fusion **59**-1 (2017) 014017.

[5] STEFANIKOVA, E., *et al*., "Effect of the relative shift between the electron density and

temperature pedestal position on the pedestal stability in JET-ILW", O4.117, EPS conference proceedings (2016), http://ocs.ciemat.es/EPS2016PAP/pdf/O4.117.pdf.

[6] SCHNEIDER, R., *et al*., “B2-EIRENE simulation of ASDEX and ASDEX-Upgrade scrape-off layer plasmas”, J. Nucl. Mater. **196** (1992) 810.

[7] WIESEN, S., *et al*., "The new SOLPS-ITER code package", J. Nucl. Mater. **463** (2015) 480-484.

[8] BONNIN, X., *et al*., "Presentation of the New SOLPS-ITER Code Package for Tokamak Plasma Edge Modeling", Plasma Fusion Research **11** (2016) 1403102.

[9] MURAKAMI, M., *et al*., "Off-axis neutral beam current drive for advanced scenario development in DIII-D", Nucl. Fusion **49** (2009) 065031.

[10] GROEBNER, R.J., OSBORNE, T.H., “Scaling studies of the high mode pedestal”, Phys. Plasmas, **5** (1998) 1800.

[11] POTZEL, S., *et al*. Nuclear Fusion **54** (2014) 013001.

[12] DUNNE, M., et al. "The role of the density profile location on pedestal stability in ASDEX Upgrade", Preprint: 26th IAEA Fusion Energy Conference, EX/3-5.

[13] MAINGI, R., et al., Phys. Rev. Lett. **107** (2011) 145004.

[14] BELL, M., et al. Plas. Phys. Cont. Fusion, **51** (2009).

[15] LOARTE, A., "Effects of divertor geometry on tokamak plasmas", Plas. Phys. Cont. Fusion, **43** (2001) R183.

[16] LOARTE, A., *et al*., Nucl. Fusion **47** (6) (2007) S203–S263.

[17] MOSER, A. L., *et al.* 22nd Int. Conf. on Plasma Surface Interactions (2016) Rome.

[18] GUO, H. Y., *et al*. Nucl. Fusion **56** (2016) 126010.

[19] ST. JOHN, H., et al., Proceedings of the Conference on Controlled Fusion and Plasma Physics, Lisboa, 1993 (European Physical Society, Geneva, 1993), Vol. 1, p. 99.

[20] MAINGI, R. *et al*., Nuclear Fusion **39** (1999) 1187.

[21] MAINGI, R. *et al*., Nuclear Fusion **44** (2004) 909.

[22] SANG, C.F., *et al*., Plas. Phys. Cont. Fusion, **59** (2017) 025009.

[23] REIMOLD, F., WISCHMEIER, M., *et al.,* "The high-field side high density region in SOLPS-modeling of nitrogen-seeded H-modes in ASDEX Upgrade", submitted to *Nucl. Mater. Energy* (2016)

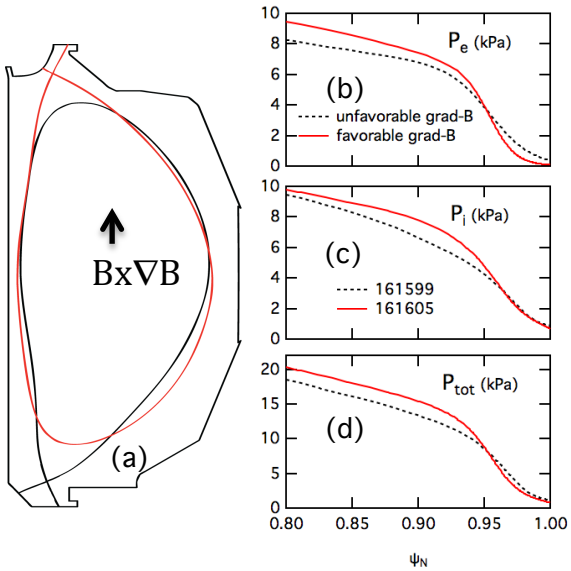

Figure 1: Comparison of pedestal pressures for discharges with opposing ∇B drift directions. The discharge shown in red (161605) has favorable ∇B drift direction while the discharge shown in black (161599) has unfavorable ∇B drift direction. Shown are (a) the last closed flux surface shapes, (b) electron pressure, (c) ion pressure and (d) total pressure.

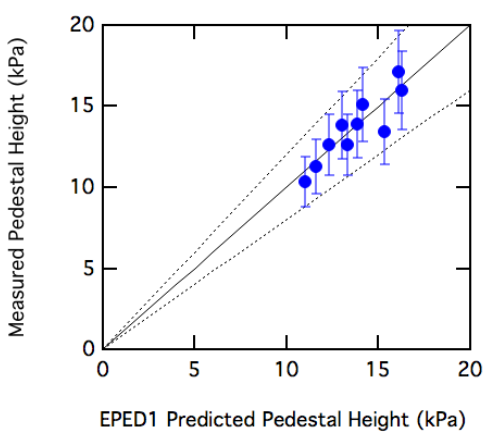

Figure 2: EPED1 predictions vs measured pedestal heights for several DIII-D discharges with ITER similar shape.

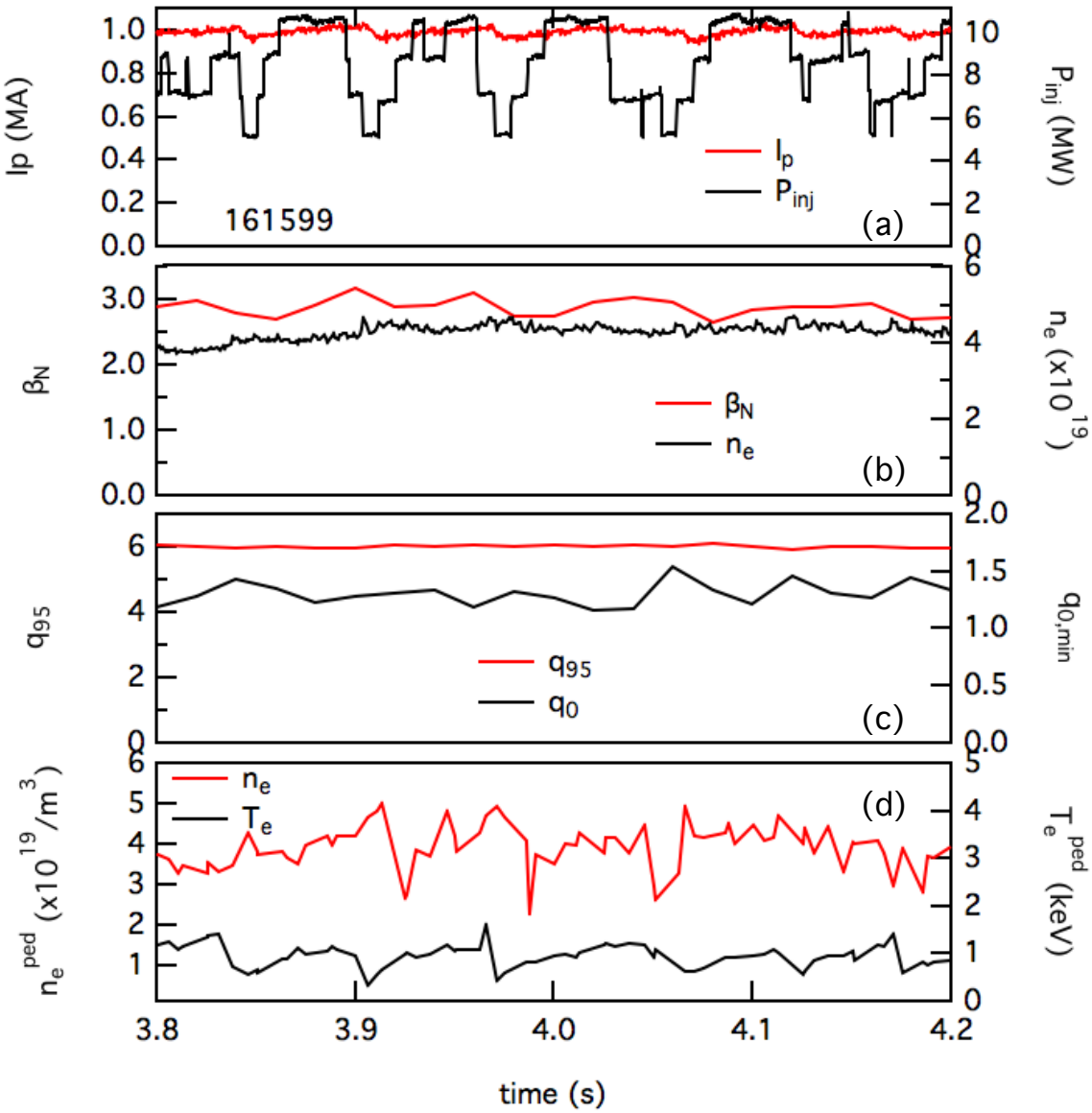

Figure 3: Time traces for shot 161599 during period of profile evaluation showing (a) plasma current and injected power, (b) normalized β and line averaged electron density, (c) q_{95} and q_0 and (d) pedestal density and electron temperature.

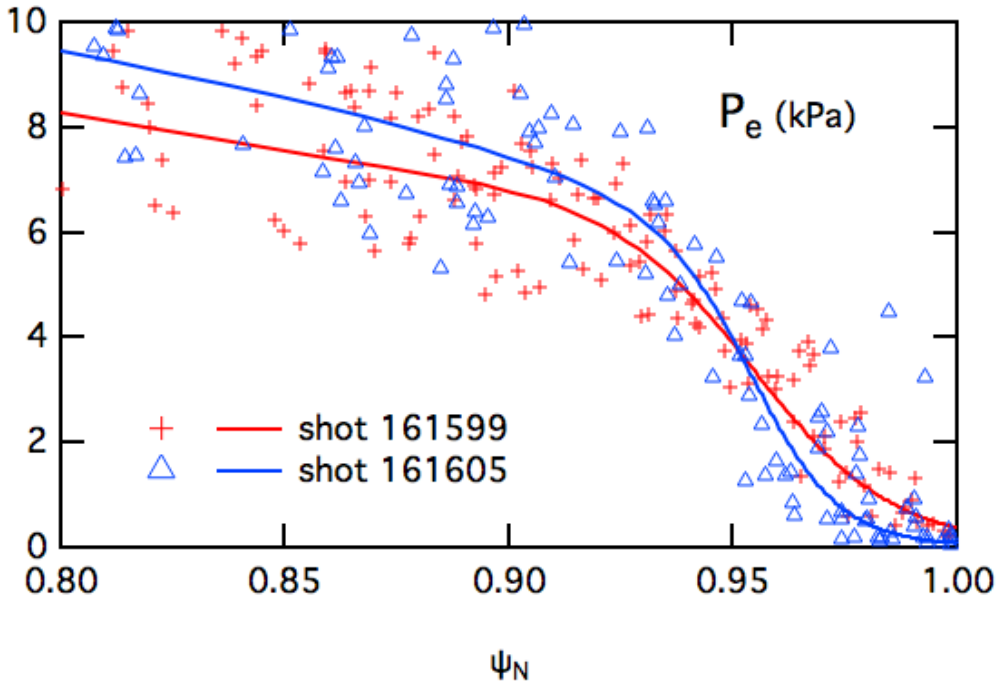

Figure 4: ELM-synched electron pressure profile fits (solid lines) and data for shot 161599 (red crosses) and shot 161604 (blue triangles).

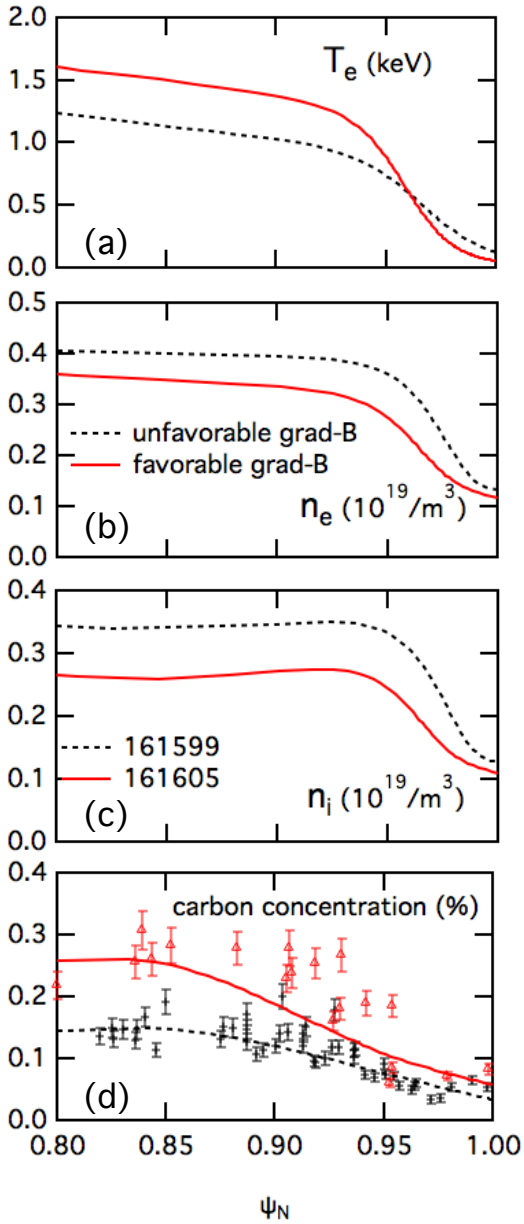

Figure 5: Experimentally fit ELM-synched pedestal profiles showing differences in (a) electron temperature, (b) electron density and (c) ion density and (d) carbon concentration between plasmas with favorable vs. unfavourable ∇B drift direction.

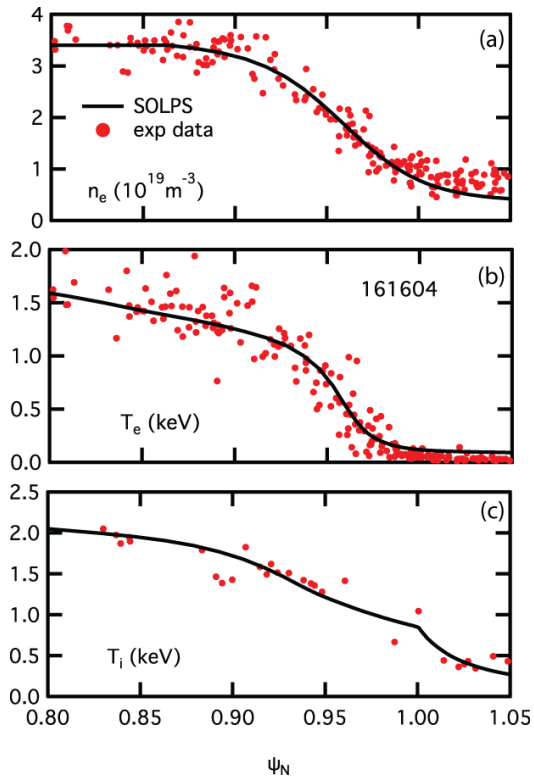

Figure 6: Comparison of SOLPS model profiles without drift effects and experimental data for shot 161604 (USN) showing (a) density, (b) T_e and (c) T_i. The electron data were obtained via Thomson scattering and the ion data were obtained via CER spectroscopy measurements.

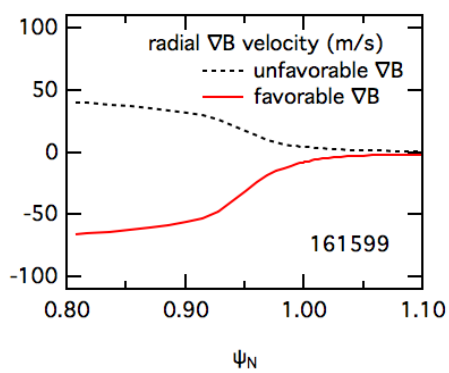

Figure 7: SOLPS calculated radial ∇B driven flow velocity at the midplane for both favorable and unfavorable ∇B drift direction. Positive flow is radially inward and negative is outward.

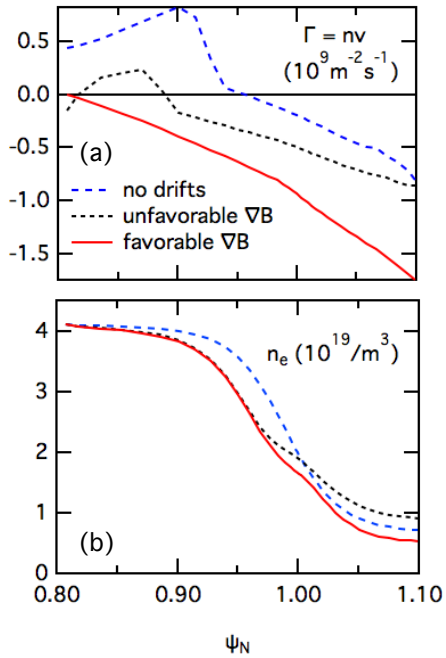

Figure 8: (a) SOLPS calculated radial particle fluxes, and (b) SOLPS calculated density profiles at the midplane for shot 161599 comparing the case with no drifts that matches the experimentally measured profiles to the cases with ∇B drifts included in forward and reverse B_T. The same transport coefficients are used for all cases.

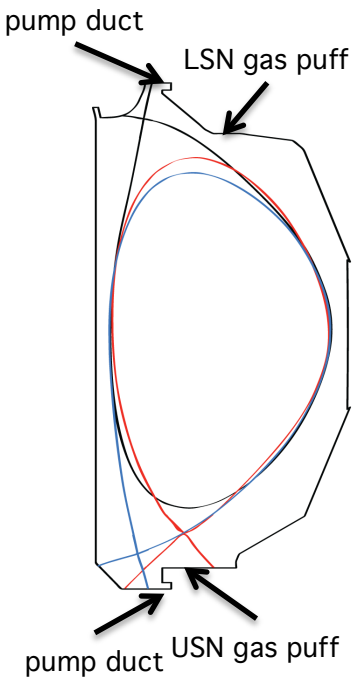

Figure 9: Separatrix geometry of the three magnetic configurations used to study the effects of divertor closure.

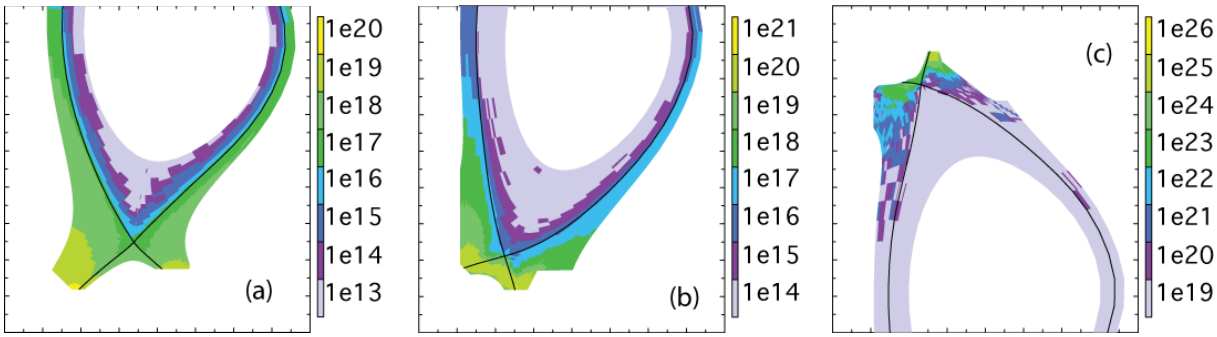

Figure 10: SOLPS calculated neutral density in particles/m^3 for: (a) the shelf configuration with least closure (shot 163250), (b) the floor configuration with intermediate closure (shot 163263) and (c) USN configuration with the greatest closure (shot 162952).

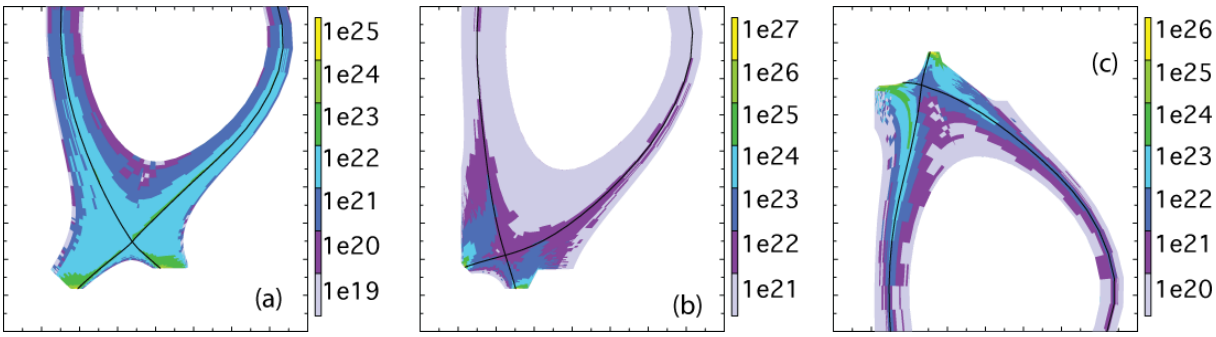

Figure 11: SOLPS calculated deuterium ionization rate in particles/m^3/s for attached plasmas in: (a) the shelf configuration with least closure (shot 163241), (b) the floor configuration with intermediate closure (shot 163259) and (c) USN configuration with the greatest closure (shot 162944).

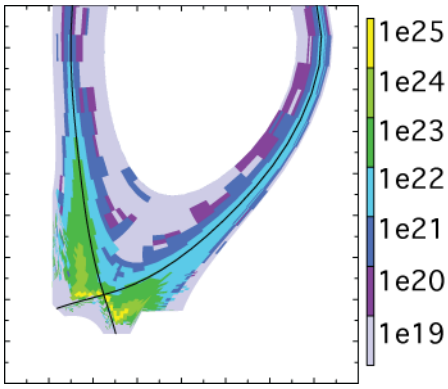

Figure 12: SOLPS calculated deuterium ionization rate in particles/m^3/s for a detached plasma in the floor configuration (shot 163263).

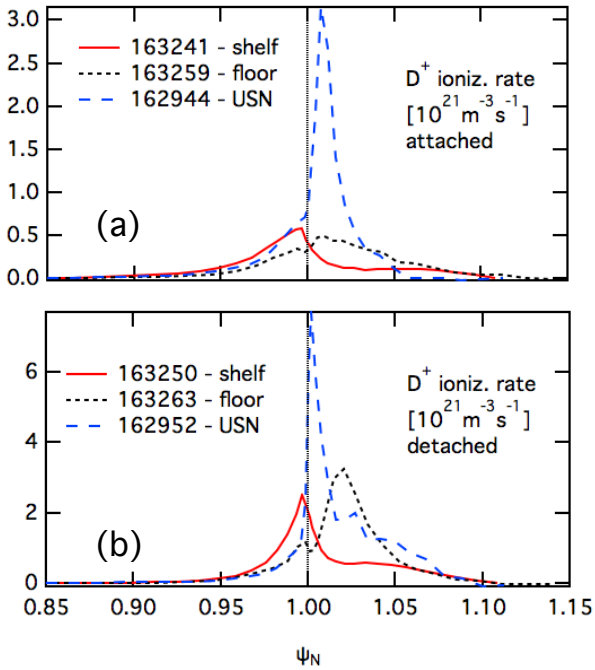

Figure 13: SOLPS calculated poloidally averaged deuterium ionization profiles for all three divertor geometries in (a) attached and (b) detached plasmas.

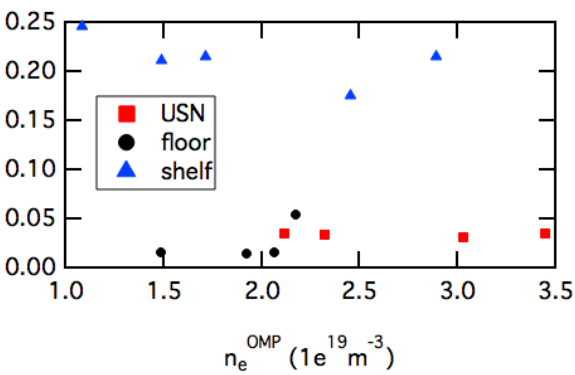

Figure 14: SOLPS calculation of fraction of total ionization that occurs within the core (at $\psi_N < 1$) vs. density for all magnetic configurations.

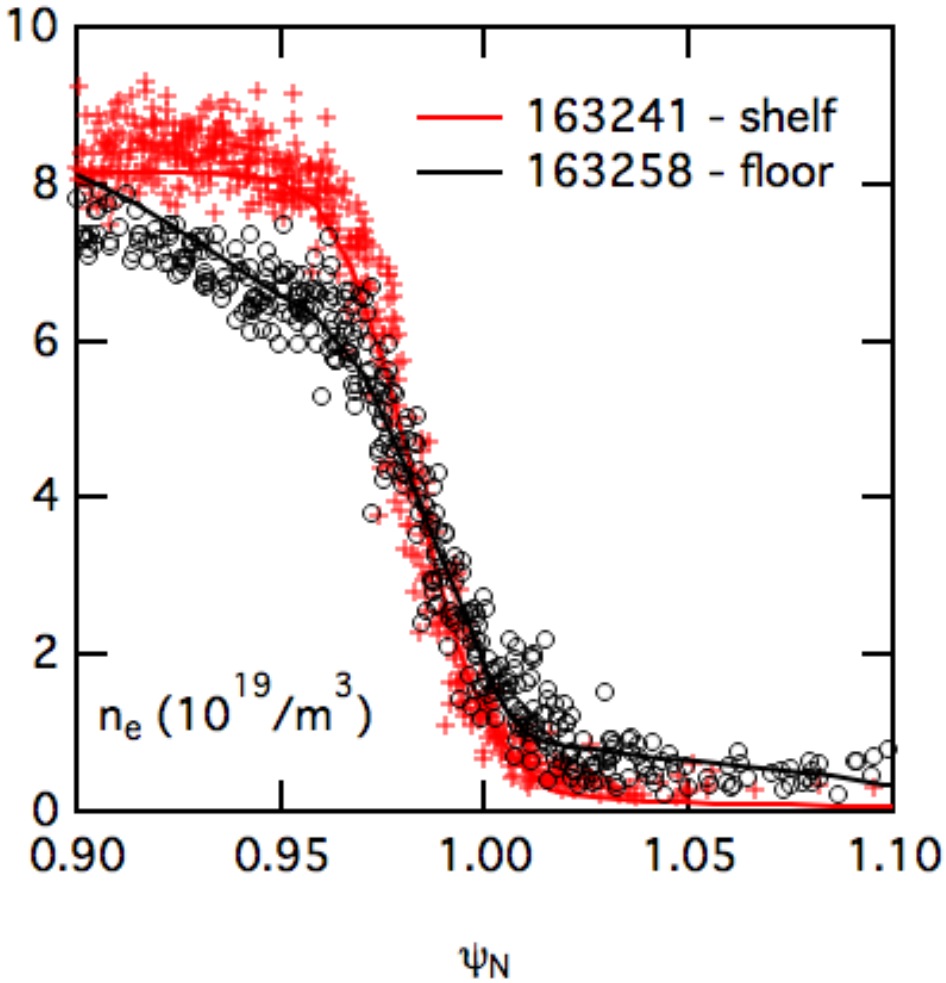

Figure 15: Comparison of the pedestal electron density profiles for the attached shelf and floor cases. The solid lines are the SOLPS profiles while the symbols are the experimental Thomson scattering data. Both cases have zero additional gas puffing.